Crystal Structure and Vibrational Spectra of $AlVO_4$. A DFT Study

Veronika Brázdová, M. Verónica Ganduglia-Pirovano, and Joachim Sauer*

Humboldt Universität zu Berlin, Institut für Chemie, Unter den Linden 6, D-10099 Berlin, Germany

Received: September 1, 2004

We present periodic density functional calculations within the generalized gradient approximation (Perdew−Wang 91) on structure and vibrational properties of bulk $AlVO_4$. The optimized structure agrees well with crystallographic data obtained by Rietveld refinement (the mean absolute deviation of bond distances is 0.032 Å), but the deviations are larger for the lighter oxygen atoms than for the heavier Al and V atoms. All observed bands in the Raman and IR spectrum have been assigned to calculated harmonic frequencies. Bands in the 1020−900 cm^{-1} region have been assigned to $V-O^{(2)}$ stretches in $V-O^{(2)}-Al$ bonds. The individual bands do not arise from vibrations of only one bond, not even from vibrations of several bonds of one VO_4 tetrahedron. The results confirm that vibrations around 940 cm^{-1} observed for vanadia particles supported on thin alumina film are V−O−Al interface modes with 2-fold coordinated oxygen atoms in the $V-O^{(2)}-Al$ interface bonds.

I. Introduction

$AlVO_4$ is the only stable ternary compound in the $V_2O_5 + Al_2O_3$ system.[1] The unit cell parameters were determined by X-ray diffraction,[2,3] and it was concluded that the compound is isostructural with $FeVO_4$. In two recent investigations atomic positions were obtained from powder diffraction data using simulated annealing[4] and the Rietveld method.[5] The first infrared spectrum was reported by Baran and Botto,[2] and complementary Raman spectra were published by Hardcastle and Wachs[6] and Briand et al.[7]

$AlVO_4$ can be used as a material for selective and sensitive sensors for detection of NO and NO_2 gases.[8,9] In addition, $AlVO_4$ represents a reference compound for vanadia catalysts supported on alumina.[7,11,17] Most catalysts based on vanadium oxides consist of a vanadium oxide phase deposited on the surface of an oxide support, such as SiO_2, TiO_2, and Al_2O_3 (ref 12). The knowledge of the local structural environment of the active *supported* vanadium sites is important for understanding their chemical properties that are relevant in heterogeneous catalysis. In this context, investigating the structural and vibrational properties of model catalyst and reference compounds that contain the same atom types as those present at the interface may be useful in the elucidation of structures of more complex systems.

Vibrational spectroscopy is a useful tool for characterization of the bonds present in the system,[6,7,10,13−15] however, the interpretation of the measured spectra is not always straightforward and needs support from quantum calculations, as a recent study of vanadium oxide supported on SiO_2 and Al_2O_3 shows.[10] The purpose of this work is to calculate the equilibrium structure and the vibrational frequencies of $AlVO_4$ by density-functional theory (DFT) applying periodic boundary conditions. The calculated frequencies are compared with the bands observed in IR[8] and Raman[6,7,16] studies of $AlVO_4$ films and $AlVO_4$ powders. The observed bands are assigned to normal modes and their relation to coordination types and bond distances is discussed. Comparison will be made with V−O−Al interface modes in recently measured IR spectra[17] of vanadia particles deposited on alumina.

II. Methods

We applied DFT with the exchange-correlation functional of Perdew and Wang (PW91)[18,19] and used a plane-wave basis set to calculate equilibrium structures. The core electrons were described by the projector augmented-wave method (PAW)[20,21] with core radii of 1.90 and 2.30 Bohr for Al and V, respectively. The 3p states of V were treated as valence states. For oxygen, core radii of 1.20 and 1.52 Bohr were used for the s and p states, respectively. The Brillouin zone was sampled using Monkhorst−Pack grids.[22] We used the Vienna ab initio simulation package (VASP).[23,24] The refined structure determined by Coelho[4] was taken as a starting point. The cell parameters as well as the internal coordinates were simultaneously optimized by a stress tensor calculation. All calculations were performed at an energy cutoff of 800 eV and used a $(2 \times 2 \times 2)$ *k*-point mesh. Tests performed at a cutoff of 400 eV show that a change from a $(2 \times 2 \times 2)$ to a $(3 \times 3 \times 3)$ *k*-point mesh results in a change of 3 meV (0.001%) in the total energy per unit cell, calculated at the experimental volume and fractional coordinates. The cutoff of 800 eV had been tested for bulk V_2O_5 (ref 25) and found sufficiently accurate to allow optimization of unit cells of vanadium containing systems. The system is an insulator and therefore the tetrahedron method with Blöchl corrections[26] was used for summation over occupied states in the reciprocal space.

The vibrational analysis was done by finite differences, with the atomic displacement set to 0.02 Bohr at the 800 eV cutoff. The vibrational modes were visualized using Molekel 4.2.[27,28]

III. Description of the $AlVO_4$ Structure

The $AlVO_4$ crystal unit cell is triclinic, space group $P\bar{1}$. There are 18 symmetry-inequivalent atoms in one unit cell. The total number of atoms in the unit cell is 36. Both crystallographic data[4,5] and a NMR study[29] showed that the unit cell contains three symmetry-inequivalent VO_4 tetrahedra, two symmetry-inequivalent AlO_6 octahedra, and one AlO_5 polyhedron (see Figure 1).

10.1021/jp046055v CCC: $30.25
Published on Web 12/10/2004

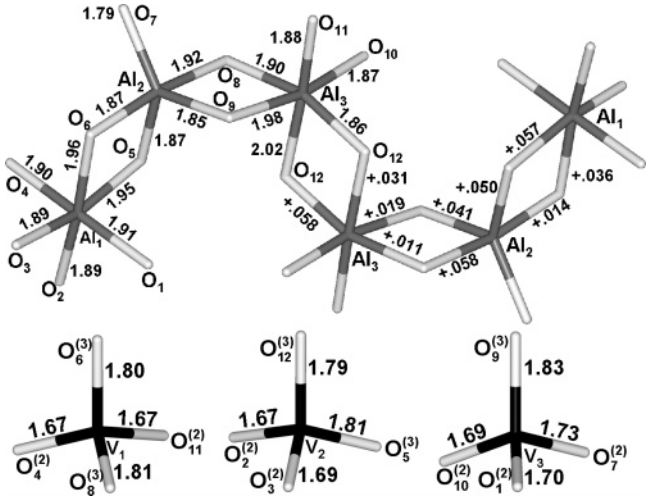

Figure 1. Coordination polyhedra of $AlVO_4$. Top: AlO_x polyhedra. Annotation on the left part of the figure: calculated bond lengths. Annotation on the right part of the figure: difference between calculated and experimental[5] bond lengths in the Al−O rings. Bottom: VO_4 polyhedra. All values are in Å.

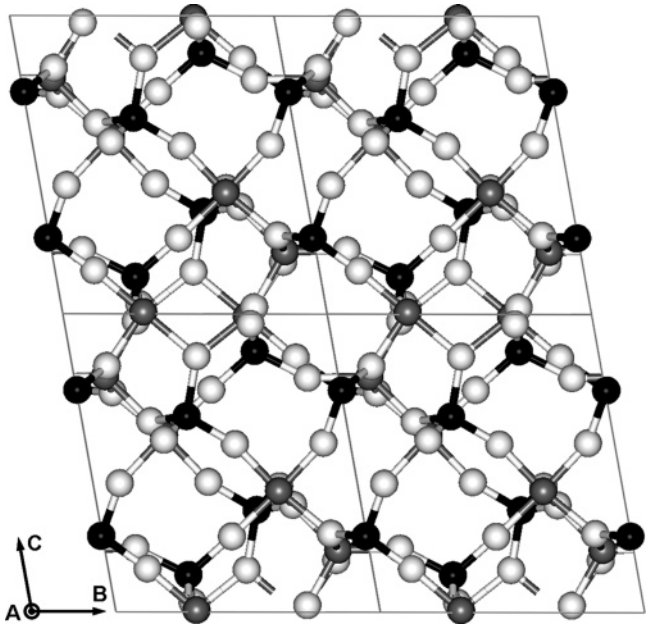

Figure 2. Structure of $AlVO_4$. The Al, V, and O atoms are depicted in gray, black, and white, respectively.

The system contains 2- and 3-fold coordinated O atoms, denoted here $O^{(2)}$ and $O^{(3)}$, respectively. There are Al−$O^{(2)}$−V bonds but no V−$O^{(2)}$−V bonds and no Al−$O^{(2)}$−Al bonds. The system does have Al−$O^{(3)}$−Al and Al−$O^{(3)}$−V bonds; i.e., the $O^{(3)}$ atoms have two bonds to Al and one bond to a V atom. No O atom is bound to three Al atoms. This is different from α-Al_2O_3, which only contains tricoordinated oxygen atoms; i.e., in α-Al_2O_3 each O atom is bound to three Al atoms. As a consequence of the characteristics listed above, each O atom in $AlVO_4$ is bound exactly to one vanadium atom. The structure contains rings, composed of alternating metal and O atoms (see Figure 2). Most of the rings contain two Al, two V, and four O atoms and will be denoted 4-rings (see Figure 3). In each ring the V and Al atoms are placed each at opposite positions of the 4-ring; i.e., the metal atoms are alternating in the ring. Twelve inequivalent 4-rings can be identified, from which there is one ring containing only 2-fold coordinated O atoms, two rings with 3 $O^{(2)}$ and 1 $O^{(3)}$, six rings with 2 $O^{(2)}$and 2 $O^{(3)}$ and three rings

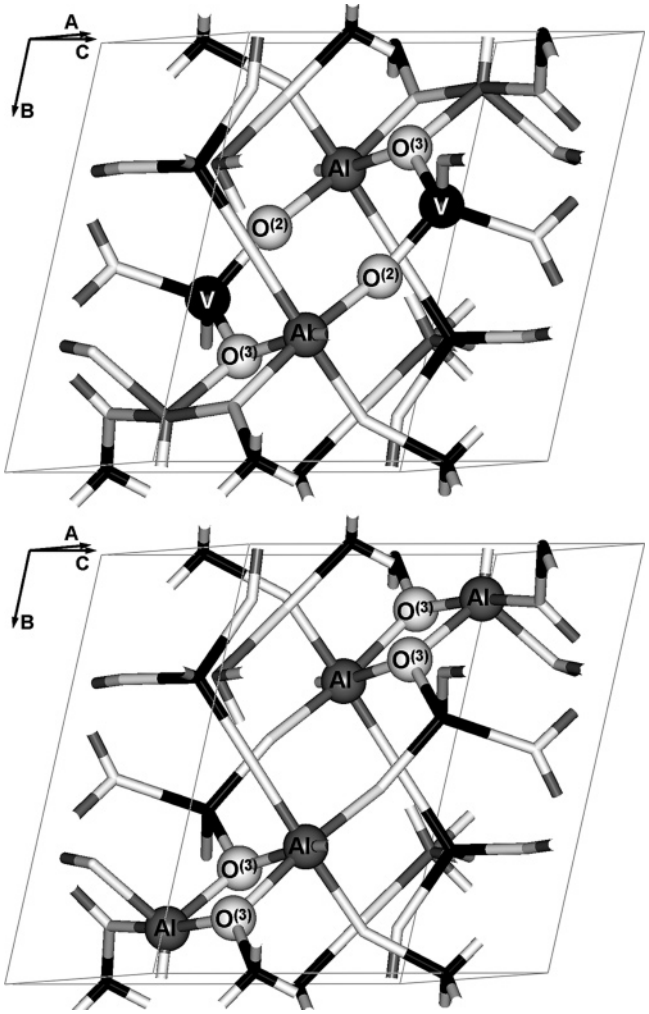

Figure 3. A 4-ring (top) and 2-rings (bottom) in the $AlVO_4$ structure. The 4-ring contains Al, V, $O^{(2)}$, and $O^{(3)}$ atoms, the 2-rings contain Al and $O^{(3)}$ atoms, drawn as "balls and sticks." The Al, V, and O atoms are depicted in gray, black, and white, respectively.

TABLE 1: Lattice Parameters of $AlVO_4$

method	a (Å)	b (Å)	c (Å)	α (deg)	β (deg)	γ (deg)	vol (Å^3)
exp[a]	6.5414	7.7598	9.1357	96.184	107.238	101.401	427.26
exp[b]	6.538	7.756	9.131	96.17	107.23	101.40	426.63
DFT/PW91[c]	6.600	7.831	9.248	96.20	107.24	101.55	440.03

[a] Reference 4. [b] Reference 5. [c] This work.

with 1 $O^{(2)}$ and 3 $O^{(3)}$ atoms. The structure also contains rings consisting of two Al and two $O^{(3)}$ atoms, which will be called 2-rings (Figure 3). There are three inequivalent 2-rings in a unit cell. Every tricoordinated O atom belongs to a 2-ring.

IV. Results and Discussion

A. Structure. Table 1 shows the optimized cell parameters, which differ from the observed values by about 1%. Table 2 shows the calculated fractional coordinates. For the heavier atoms Al and V the atomic positions agree well with the experimental data of Coelho (Table 3 of ref 4) and Arisi et. al (Table 3 of ref 5; note that these authors number the O sites differently). The deviation from the experimental fractional coordinates is larger for some O atoms, especially when compared with the data from ref 4, e.g., O_3, O_4, or O_{11} atoms. As a result some V−O and Al−O bond lengths differ by up to 0.12 Å (ref 4) and up to 0.06 Å (ref 5), respectively. The standard deviations of the calculated bond distances from the

TABLE 2: Optimized Fractional Coordinates of Crystalline $AlVO_4$

atom	*x*	*y*	*z*
Al_1	0.74876	0.69900	0.40740
Al_2	0.46078	0.88231	0.20944
Al_3	0.96312	0.30658	0.00745
V_1	0.99685	0.00424	0.74493
V_2	0.19556	0.60025	0.34260
V_3	0.51678	0.29922	0.12450
O_1	0.64155	0.48978	0.25411
O_2	0.25602	0.43673	0.43636
O_3	0.04045	0.70137	0.42205
O_4	0.15898	0.10058	0.43155
O_5	0.45684	0.74194	0.35973
O_6	0.75095	0.86522	0.26396
O_7	0.52185	0.11686	0.21378
O_8	0.15589	0.86776	0.17458
O_9	0.35368	0.72829	0.02333
O_{10}	0.25224	0.29613	0.03252
O_{11}	0.95151	0.14930	0.14614
O_{12}	0.05005	0.52211	0.14179

observed ones are 0.051 and 0.036 Å for refs 4 and 5, respectively. Table 3 lists calculated bond lengths and their deviation from the two sets of experimental data. Compared to ref 4, longer V−O bonds are compensated for by shorter Al−O bonds. This is reflected in the average values of the deviations for the VO_4 tetrahedra and AlO_x polyhedra, which are also given in Table 3. The largest differences are in V−O−Al bridges involving $O^{(2)}$ atoms, $V_2-O_3^{(2)}-Al_1$ (+0.101 Å; −0.062 Å), $V_1-O_4^{(2)}-Al_1$ (+0.084 Å; −0.054 Å), and $V_1-O_{11}^{(2)}-Al_3$ (+0.117 Å; −0.083 Å) bond lengths. Smaller deviations are seen for $V_3-O_7^{(2)}-Al_2$ (+0.075 Å; −0.027 Å) and $V_3-O_{10}^{(2)}-Al_3$ (+0.049 Å; −0.024 Å) bonds. The deviations for the $Al-O^{(3)}$ bonds are also not negligible (up to 0.084 Å).

The agreement with the more recent refinement of ref 5 is better and the average deviations for individual polyhedra are closer to zero. Figure 1 shows the calculated bond distances and their deviations from the experimental values of ref 5 for the three AlO_x polyhedra and the three VO_4 tetrahedra. There is still some compensation in V−O−Al bridges between too long and too short bonds, in particular for bonds that show the largest deviations, e.g., $V_2-O_5^{(3)}-Al_1$ (−0.064 Å; +0.057 Å), $-O_5^{(3)}-Al_2$ (+0.050 Å), and $V_1-O_4^{(2)}-Al_1$ (+0.031 Å; −0.056 Å). Figure 4 shows the calculated bond distances and their deviations from the experimental values of ref 5 for the twelve inequivalent 4-rings. The alternation of too long V−O bonds

TABLE 3: $AlVO_4$ Bond Lengths and the Differences Δ between the Calculated and Experimental Values (All Values in Å)

		DFT[a]	Δ[b]	Δ[c]			DFT	Δ[b]	Δ[c]
V_1	$-O_4^{(2)}$	1.665	+0.078	+0.041	Al_1	$-O_1^{(2)}$	1.906	−0.005	+0.053
	$-O_6^{(3)}$	1.800	−0.015	+0.023		$-O_2^{(2)}$	1.888	−0.012	−0.024
	$-O_8^{(3)}$	1.807	−0.004	−0.023		$-O_3^{(2)}$	1.886	−0.062	−0.024
	$-O_{11}^{(2)}$	1.673	+0.117	−0.013		$-O_4^{(2)}$	1.904	−0.054	−0.056
						$-O_5^{(3)}$	1.951	−0.016	+0.057
						$-O_6^{(3)}$	1.957	+0.036	+0.036
average		1.736	+0.048	−0.004	average		1.915	−0.013	−0.007
V_2	$-O_2^{(2)}$	1.670	−0.016	+0.031	Al_2	$-O_5^{(3)}$	1.866	+0.058	+0.050
	$-O_3^{(2)}$	1.691	+0.101	+0.041		$-O_6^{(3)}$	1.867	+0.040	−0.014
	$-O_5^{(3)}$	1.807	+0.032	−0.064		$-O_7^{(2)}$	1.793	−0.027	−0.016
	$-O_{12}^{(3)}$	1.791	−0.000	−0.009		$-O_8^{(3)}$	1.919	−0.010	+0.058
						$-O_9^{(3)}$	1.846	−0.032	+0.041
average		1.740	+0.037	−0.000	average		1.858	−0.006	+0.029
V_3	$-O_1^{(2)}$	1.697	+0.040	+0.028	Al_3	$-O_8^{(3)}$	1.899	+0.084	−0.011
	$-O_7^{(2)}$	1.726	+0.075	+0.025		$-O_9^{(3)}$	1.982	+0.023	+0.019
	$-O_9^{(3)}$	1.830	−0.003	−0.009		$-O_{10}^{(2)}$	1.872	−0.024	−0.010
	$-O_{10}^{(2)}$	1.694	+0.049	+0.021		$-O_{11}^{(2)}$	1.879	−0.083	+0.041
						$-O_{12}^{(3)}$	1.860	+0.048	+0.058
						$-O_{12}^{(3)}$	2.021	+0.022	+0.031
average		1.737	+0.042	−0.016	average		1.919	−0.012	+0.028

[a] This work. [b] Reference 4, [c] Reference 5.

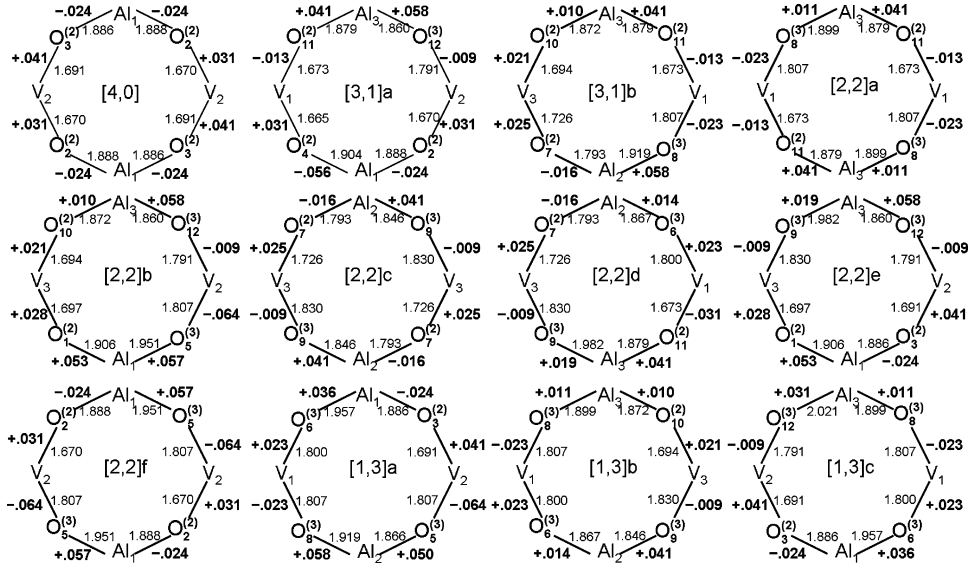

Figure 4. Bond length differences (Å) between the calculated and experimental[5] values. The bond lengths given are the values calculated in this work. The labeling of the rings shows the number of $O^{(2)}$ and $O^{(3)}$ atoms in a ring, [number of $O^{(2)}$, number of $O^{(3)}$].

TABLE 4: Experimental and Calculated V−O(2)−Al Stretching Modes of $AlVO_4$

type	IR[a]	Raman[a]	Raman[b]	Raman[c]	DFT[d]
IR	1013				1025
Raman		1017	1017	1020/1013[e]	1007
Raman		988	988	991/992[e]	974
IR	969				973
IR					946
Raman		952	949	954	943
IR					940
Raman				[954]	939
IR	919				925
Raman		919	919	925	909
Raman		901	899	907	901
IR	892				900
Raman		[901][f]	[899]	[907]	895
IR	[892]				882

[a] Reference 8. Thin $AlVO_4$ film supported on a ceramic corundum substrate. [b] Reference 6. Powder $AlVO_4$. [c] Reference 7. Powder $AlVO_4$. [d] This work. [e] The second value was obtained with grating 2400 grooves/mm. Reference 16. [f] Values in square brackets indicate where a unique assignment of observed frequencies to calculated ones could not be made.

and too short Al−O bonds is obvious. The (mean absolute) deviations of the calculated bond distances from the observed ones (0.040 and 0.032 Å for refs 4 and 5, respectively) are somewhat larger than expected for the computational method used here (DFT/PW91), at least in case of comparison with ref 4. Calculated distances for the vanadyl bond in the gas-phase $VOCl_3$ molecule (1.59 Å, this work) or in crystalline vanadium pentoxide[25,30] are consistently larger by 0.01−0.02 Å than observed values.[31,32] On the basis of the closer agreement with the DFT calculations we conclude that the atomic positions obtained by Rietveld refinement[5] are more accurate than the coordinates obtained by simulated annealing.[4] The deviation pattern for neighbouring bonds indicates that even between the Rietveld refinement[5] and the DFT calculations, the deviations are larger for the lighter O atoms than for the heavier Al and V atoms. This may reflect that DFT calculations determine equilibrium positions of atoms whereas experimentally the thermal and vibrational average of the atom positions is obtained.

B. Vibrational Properties. The point group of the $AlVO_4$ crystal is C_i, which means that its vibrational modes belong to the A_g and A_u irreducible representations. Out of the 105 optical modes 54 A_g modes are Raman active and 51 A_u modes infrared active. The three acoustic modes belong to A_u. Pairs of A_g and A_u modes that are close in energy should correspond to similar vibrations, with the main difference in the relative phase of the individual atomic moves. This is indeed the case especially for stretching modes with the highest frequencies. For the lower frequency bending modes strong coupling makes such an analysis difficult. The assignment to experimental frequencies within a given irreducible representation is based on the sequence of wavenumbers. The cases for which an unambiguous assignment could not be made are indicated. Tables 4−8 list the calculated and observed frequencies for different wavenumber ranges and different types of vibrations:

(a) 1025−880 cm^{-1}: V−O(2)(−Al) stretching

(b) 860−670 cm^{-1}: V−O(−Al) stretching and distortion of 2-rings

(c) 590−400 cm^{-1}: Al−O stretching and Al−O(2)−V and Al−O(3)−Al bending

(d) 400−170 cm^{-1}: bending modes, all polyhedra distorted

(e) below 170 cm^{-1}: bending modes, rigid polyhedra.

In the following description of the vibrations the wavenumbers specified refer to Raman active modes, the numbers in parentheses correspond to the IR active modes.

(a) The highest vibrations above 895 (882) cm^{-1} correspond to stretching modes of V−O(2) bonds in 4-rings, whereas O(3) atoms in the 2-rings remain undistorted. The three highest pairs

TABLE 5: Experimental and Calculated Vibrational Modes of $AlVO_4$ Involving Al−O and V−O Stretching and Distortion of 2-rings

type	IR[a]	Raman[a]	Raman[b]	Raman[c]	DFT[d]
Raman		854	850	858	833
IR					832
Raman				822	805
IR					793
Raman				785	790
IR	719				735
IR	[719][e]				706
Raman				710	704
IR					678
Raman				670	667

[a] Reference 8. Thin $AlVO_4$ film supported on a ceramic corundum substrate. [b] Reference 6. Powder $AlVO_4$. [c] Reference 7. Powder $AlVO_4$. [d] This work. [e] Value in square brackets indicates where a unique assignment of observed frequencies to the calculated one could not be made.

TABLE 6: Experimental and Calculated Vibrational Modes of $AlVO_4$ Involving Al−O Stretching and Al−O(2)−V and Al−O(3)−Al Bending Modes (All Polyhedra Distorted)

type	IR[a]	Raman[a]	Raman[b]	Raman[c]	DFT[d]
Raman				569/572[e]	587
IR	617				582
Raman			557	[521/544[e]]	552
IR	588				552
Raman				521/514[e]	544
IR	537				535
Raman		518	510	[466]	516
IR					511
IR					501
Raman				466[f]	496
IR					481
Raman				405[f]	460
Raman				405[f]	450
IR	461				449
Raman				405[f]	442
IR					442
Raman				405[f]	434
IR	428				426
IR	[428][g]				425
Raman				405[f]	422
IR					418

[a] Reference 8. Thin $AlVO_4$ film supported on a ceramic corundum substrate. [b] Reference 6. Powder $AlVO_4$. [c] Reference 7. Powder $AlVO_4$. [d] This work. [e] This value was obtained with grating 2400 grooves/mm. Reference 16. [f] Broad peak in observed spectrum; see Figure 6. [g] Value in square brackets indicates where a unique assignment of observed frequencies to the calculated one could not be made.

TABLE 7: Experimental and Calculated Bending Modes of $AlVO_4$ (All Polyhedra Distorted)

type	Raman[a]	Raman[b]	DFT[c]
IR			407
Raman		405[d]	415, 409, 407
IR			401, 391
Raman		382[d]	388, 384, 377
IR			367
Raman	371	382[d]	367
IR			364, 357
Raman		382[d]	357, 350
IR			343, 334
Raman	319	329[d]	331, 322, 317, 309, 300
IR			329, 323, 309, 296, 299, 292
Raman	279	288[d]	290, 281, 275
IR			280, 268, 253

[a] Reference 6. Powder $AlVO_4$. [b] Reference 7. Powder $AlVO_4$. [c] This work. [d] Broad peak in observed spectrum; see Figure 6.

TABLE 8: Experimental and Calculated Vibrational Modes of $AlVO_4$ Involving Distortion of 4- and 2-Rings, with Rigid Polyhedra (below 170 cm^{-1}) and with Slightly Distorted Polyhedra (above 170 cm^{-1})

type	Raman[a]	Raman[b]	DFT[c]
IR			247
Raman		242	242, 233
IR			238, 218
Raman	215	226	216, 208, 203
IR			211, 193
Raman		192	188, 180, 170, 165, 149, 146
IR			178, 165, 161, 145, 138, 136
Raman	133		134
Raman			126, 115, 100

[a] Reference 6. Powder $AlVO_4$. [b] Reference 7. Powder $AlVO_4$. [c] This work.

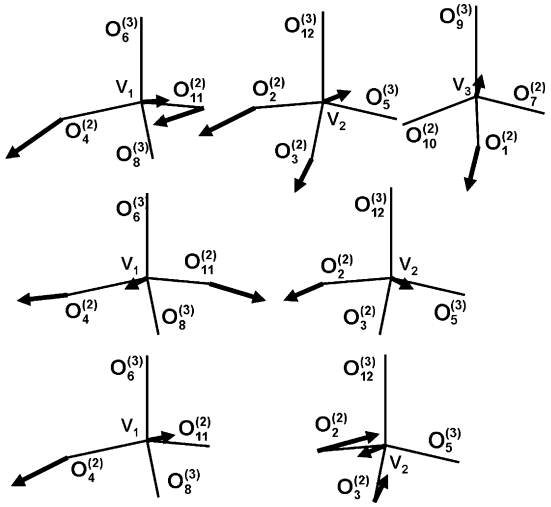

Figure 5. V−O bonds involved in the two highest Raman vibrations, at 1007 cm^{-1} (top), at 974 cm^{-1} (middle), and at 943 cm^{-1} (bottom).

of vibrations at 1007 (1025), 974 (973), and 943 (946) cm^{-1} couple stretching motions of different selections from the two shortest bonds in each of the three VO_4 tetrahedra as found by inspection of the calculated normal modes. Figure 5 shows the normal modes for the Raman active vibrations at 1007, 974, and 943 cm^{-1}. The 1007 cm^{-1} vibration is dominated by coupled stretches of the two shortest $V-O^{(2)}$ bonds in the V_1 and V_2 tetrahedra ($V_1-O_4^{(2)}$ (1.665 Å), $V_1-O_{11}^{(2)}$ (1.673 Å), $V_2-O_2^{(2)}$ (1.670 Å), $V_2-O_3^{(2)}$ (1.691 Å)), and of one of the two shorter bonds of the V_3 tetrahedron, $V_3-O_1^{(2)}$ (1.697 Å). The 974 cm^{-1} normal mode is a coupling of stretches of the two shortest bonds of the V_1 tetrahedron with the stretch of the shortest bond ($V_2-O_2^{(2)}$) of the V_2 tetrahedron. In the 943 cm^{-1} normal mode the shortest bond of the V_1 tetrahedron ($V_1-O_4^{(2)}$) couples with the two shortest bonds of the V_2 tetrahedron. The four pairs of vibrations with lower wavenumbers down to 895 (882) cm^{-1} include contributions from all $V-O^{(2)}$ bonds including the bonds with distances of 1.694 and 1.726 Å.

(b) The modes in the 833−667 (832−678) cm^{-1} region combine Al−O and V−O stretchings and involve also in-plane distortions of 2-rings. The O atoms move whereas the Al ions stay fixed in their equilibrium positions. For modes above 790 cm^{-1} the 2-ring distortion has the form of ring-breathing. DFT calculations for crystalline α-Al_2O_3 (corundum) predict $Al-O^{(3)}$ stretch modes in the same range,[30] the highest Raman active mode at 845 cm^{-1} and an IR active mode at 630 cm^{-1} (observed 635 cm^{-1}).[33] The α-Al_2O_3 and $AlVO_4$ structures have the three-coordinated oxygen atoms and the AlO_6 octahedra in common, but the $O^{(3)}$ oxygen atoms are coordinated only to Al atoms in

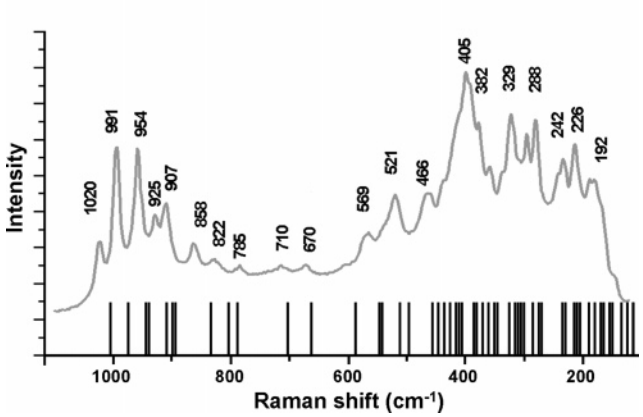

Figure 6. Comparison of the calculated frequencies of Raman active modes (vertical lines, this work) with the experimental Raman spectrum (Figure 1 of ref 7, grating 900 groves/mm).

α-Al_2O_3 (distances of 1.86 and 1.97 Å)[34] and to two Al and one V in $AlVO_4$ (Al−O distances between 1.81 and 1.99 Å; V−O distances between 1.78 and 1.87 Å).[5]

(c) In the 587−422 (582−418) cm^{-1} region bending modes occur together with stretching modes. This region is separated by a gap of 80 (96) cm^{-1} from the pure stretching vibrations of region (b). The lower the energy of the vibration, the less pronounced are the stretching modes. The 2-rings are still distorted, whereas the 4-rings remain largely unaffected. Baran and Botto[2] suggested that groups of bands can be attributed to vibrations of particular polyhedra, for example vibrations of the AlO_5 polyhedra should produce bands around 700 cm^{-1} and vibrations of the AlO_6 octahedra should give rise to bands between 500 and 600 cm^{-1}. However, we find that the vibrations of the AlO_6 octahedra and those of the AlO_5 units are coupled.

(d) In the 415−275 (407−253) cm^{-1} region the vibrational motion is a mixture of bending moves, involving bonds of both Al and V with two- and three-coordinated O atoms. Between 242 and 170 (247−178) cm^{-1} the vibrations correspond to distortions of the 4-rings. From ∼190 cm^{-1} upward the distortion affects also the 2-rings. All polyhedra are still slightly distorted.

(e) The lowest vibrations, between 165 and 100 (165−135) cm^{-1}, correspond to distortion of the 4-rings, with rigid polyhedra; i.e., all the polyhedra move as rigid units, deforming the $V-O^{(2)}-Al$ bonds. The 2-rings are only slightly distorted.

C. Comparison with Observed IR and Raman Spectra. Figure 6 compares the observed Raman spectrum[7] with the calculated spectrum shown as sticks because calculated intensities are not available. It is clearly seen that down to 466 cm^{-1} every observed Raman line can be related to one, the lines at 954, 907, 521, and 466 cm^{-1} to two, calculated Raman active normal modes (see Tables 5 and 7 for the calculated wavenumbers). The peaks below 450 cm^{-1} are due to a high density of Raman-active vibrational states. The root-mean-square (RMS) deviation[35] between the calculated and observed frequencies is 17 cm^{-1} for the observed Raman bands[6] above 460 cm^{-1}, and 20 cm^{-1} for the observed IR bands[8] above 530 cm^{-1}. Scaling of the calculated frequencies by a uniform factor[38] $f = \nu_{obsd}/\nu_{calc}$ does not improve the RMS deviation. Mean absolute errors of 66 and 42 cm^{-1} have been reported for DFT calculations on small molecules that use the PW91 and the (similar) PBE functional, respectively.[36,37] The good agreement of the calculated vibrational spectra, both IR and Raman, with the observed ones supports the calculated structure and atomic positions, because vibrational frequencies cannot be accurately predicted without having an accurate structure.

TABLE 9: Calculated Raman Frequencies and Bond Distances of V−O Bonds

compound	bond type	bond length (Å)	Raman frequency (cm^{-1})
V_2O_5	$V-O^{(3)}$	1.89	676
V_4O_{10}	$V-O^{(2)}-V$	1.80	841
V_2O_5	$V-O^{(2)}-V$	1.79	851
$AlVO_4$	$V-O^{(2)}(-Al)$	1.67, 1.68, 1.70[a]	1007, 974, 943
V_2O_5	V=O	1.59	1026

[a] Because many V−O bonds contribute to all three vibrations, we give average values for the three VO_4 tetrahedra only (see text).

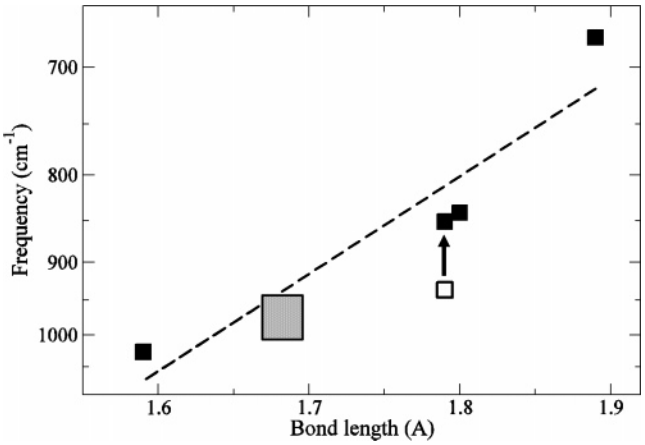

Figure 7. Dependence of Raman frequencies on bond distances of V−O bonds (see text). Data from Table 9.

D. Frequencies and Bond Distances. In the absence of reliable structure data for complex materials such as V_2O_5 catalysts supported on oxides,[10,17] one may be tempted to apply a correlation between V−O stretching frequencies available from Raman spectra and V−O bond distances to make predictions of the latter. For example, Hardcastle and Wachs[6] assigned the three highest Raman bands at 1017, 988, and 949 cm^{-1} to the shortest V−O bonds of each of the three VO_4 tetrahedra and predicted bond lengths of 1.59, 1.60, and 1.61 Å. Both the Rietveld refinement (1.62, 1.64, 1.67) and the present calculations (1.67, 1.67, 1.69) yield significantly larger distances for these bonds. The vibrational frequency−bond distance correlation is based on the "diatomic approximation", which assumes that the vibration considered is due to a single metal−oxygen bond that is vibrationally independent of the crystalline lattice. A classical case, and perhaps the only one for which this assumption is justified, are OH vibrations in molecules and on surfaces. Due to its high frequency the OH mode is well separated from crystal phonons. Moreover, the application of the frequency−bond distance correlation may be complicated by couplings between V−O vibrations of several bonds. The present DFT calculations on $AlVO_4$ and previous ones for V_2O_5 (ref 30) show the limits of the "diatomic approximation" for V−O bonds in different coordinations. Table 9 summarizes Raman frequencies and bond distances of V−O bonds in these systems, and Figure 7 shows the corresponding plot. The plot is not linear but follows the Badger rule, which assumes that the harmonic force constant is inversely proportional to the cube of the bond distance. The unit cell of V_2O_5 includes four V=O bonds, which are coupled but exhibit only a small splitting, as seen from the narrow range of calculated frequencies, 1006−1026 cm^{-1} (ref 30). The two Raman frequencies differ by 2 cm^{-1} only and there is no ambiguity in relating a frequency to a bond distance. Things are different for the $V-O^{(2)}$ bonds in V_2O_5. There are two $V-O^{(2)}-V$ bridges in the V_2O_5 unit cell and the two antisymmetric $V-O^{(2)}-V$ stretches give rise to an in-phase (B_{2g}) and antiphase (B_{3u}) mode at 936 (Raman, obsd 963) and 768 (IR, obsd 768) cm^{-1}, respectively. Both are due to the same bond distance of 1.79 Å (obsd 1.78 Å). Hence only the mean value of the two frequencies is expected to correlate with the bond distance. This is seen in Figure 7: The Raman frequency (open square) is off the (tentative) line, whereas the average of the Raman and IR frequency (full square) follows the trend much better. The present calculations for $AlVO_4$ have shown that the Raman modes at 1007, 974, and 943 cm^{-1} include contributions from the two shorter bonds of the VO_4 tetrahedra. Therefore, Table 9 shows the mean distance of the two shorter V−O bonds for the three tetrahedra. Further, the calculations revealed that all three tetrahedra (or at least two of them) are involved (Figure 5) and therefore an assignment of the Raman bands to individual tetrahedra is not possible. In Figure 7 the ranges of the frequencies and the corresponding bond lengths have been marked by the gray rectangle.

As a consequence of the couplings between different V−O bonds in V_2O_5 and $AlVO_4$ the observed Raman frequency of $V-O^{(2)}$ bonds in V_2O_5 (963 cm^{-1}) is at the low edge of the range of $AlVO_4$ values (954−1020 cm^{-1}), whereas the observed V−O distance in V_2O_5 (1.78 Å) is significantly longer than the corresponding observed distances in $AlVO_4$ (1.62−1.69 Å). Moreover, in contrast to the free vanadyl bonds in V_2O_5 the V−O bonds in $AlVO_4$ are part of V−O−Al bridges, which also affects the frequencies. The vanadyl frequency of V_2O_5 (992 cm^{-1})[39] is within the range of V−O frequencies of $AlVO_4$ (954−1020 cm^{-1}), but the vanadyl bond distance in V_2O_5 (1.58 Å)[32] is significantly shorter than the shorter V−O bonds in $AlVO_4$ (1.62−1.69 Å).[5]

The present study shows that V−O stretchings in $V-O^{(2)}-$Al bonds have vibrational frequencies between 1025 and 882 cm^{-1}. A thin V_2O_5 film supported on α-Al_2O_3, which has only tricoordinated oxygen atoms (and no 2-fold coordinated oxygen atoms), has V−O stretchings in $V-O^{(3)}(-Al)_2$ bonds up to ∼805 cm^{-1} (ref 30). This indicates that complex systems consisting of vanadia supported on alumina, with V−O−Al interface bands between 1000 and 900 cm^{-1} are very likely to have 2-fold coordinated oxygen atoms in the V−O−Al interface bonds. Recent DFT studies on cluster models[10] for vanadia on Al_2O_3 in which Al is tetrahedrally coordinated and O is 2-fold coordinated and in which $V-O^{(2)}-$Al bonds are present confirm the appearance of bands within the 955−926 cm^{-1} range. The VO_x/Al_2O_3 model catalyst consisting of vanadia particles on an alumina film[17] has a prominent band at about 940 cm^{-1}, which has been assigned to an interface mode.[10] The present calculations for $AlVO_4$ provide further support for this assignment and point to the presence of $V-O^{(2)}-$Al interface bonds. This is consistent with the presence of Al in tetrahedral sites of the Al_2O_3 film.[40−42]

V. Conclusions

The $AlVO_4$ crystal has been investigated by periodic DFT/PW91 calculations. Cell parameters and fractional coordinates obtained by DFT calculations (PW91/plane waves) agree well with crystallographic data obtained by Rietveld refinement.[5] The mean absolute deviation between calculated bond distances and the Rietveld results is 0.032 Å and a detailed analysis shows that the deviations are larger for the lighter oxygen atoms than for the heavier Al and V atoms.

The harmonic vibrational spectrum was calculated and compared with experimental results. All observed bands down to 460 cm^{-1} have been assigned to calculated vibrational transitions. The root-mean-square (RMS) deviation[35] between

calculated and observed Raman[6] and IR[8] frequencies in this range is 17 and 20 cm^{-1}, respectively. Seven pairs of IR and Raman active vibrations in the region between 1020 and 900 cm^{-1} are assigned to stretches of $V-O^{(2)}(-Al)$ bonds. However, due to couplings individual bands cannot be assigned to specific VO_4 tetrahedra. The three highest frequencies observed in the Raman spectrum[7] at 1020, 991, and 954 cm^{-1} are due to different couplings between stretches of five or three $V-O^{(2)}$ bonds out of the set of the two shortest bonds in each VO_4 tetrahedron (between 1.62 and 1.69 Å).[5] The vibrations at 925 and 907 cm^{-1} (Raman)[7] have contributions from all $V-O^{(2)}$ bonds with distances up to 1.70 Å.[5] The present results support the assignment of the 940 cm^{-1} band for vanadia particles on a thin alumina film to the V−O−Al interface mode[10,17] and at the same time hint at 2-fold coordinated oxygen in the $V-O^{(2)}-$Al interface.

Acknowledgment. This work was supported by Deutsche Forschungsgemeinschaft (Sonderforschungsbereich 546). The calculations were carried out on the IBM pSeries 690 system at HLRN. We thank I. E. Wachs for providing an electronic version of the Raman spectrum of $AlVO_4$ (ref 7) and for useful discussions.

References and Notes

(1) Burdese, A. *Ann. Chim. (Roma)* **1957**, *47*, 797−805.
(2) Baran, E. J.; Botto, I. L. *Monatsh. Chem.* **1977**, *108*, 311−318.
(3) Yamaguchi, O.; Uegaki, T.; Miyata, Y.; Shimizu, K. *J. Am. Ceram. Soc.* **1987**, *70*, C−198−C−200.
(4) Coelho, A. A. *J. Appl. Crystallogr.* **2000**, *33*, 899−908.
(5) Arisi, E.; Palomares Sánchez, S. A.; Leccabue, F.; Watts, B. E.; Bocelli, G.; Calderón, F.; Calestani, G.; Righi, L. *J. Mater. Sci.* **2004**, *39*, 2107−2111.
(6) Hardcastle, F. D.; Wachs, I. E. *J. Phys. Chem.* **1991**, *95*, 5031−5041.
(7) Briand, L. E.; Jehng, J.-M.; Cornaglia, L.; Hirt, A. M.; Wachs, I. E. *Catal. Today* **2003**, *78*, 257−268.
(8) Leyer, B.; Schmelz, H.; Göbel, H.; Meixner, H.; Scherg, T.; Knöziger, H. *Thin Solid Films* **1997**, *310*, 228−233.
(9) Ishihara, T.; Shiokawa, K.; Eguchi, K.; Arai, H. *Sens. Actuators* **1989**, *19*, 259−265.
(10) Magg, N.; Immaraporn, B.; Giorgi, J. B.; Schroeder, T.; Bäumer, M.; Döbler, J.; Wu, Z.; Kondratenko, E.; Cherian, M.; Baerns, M.; Stair, P. C.; Sauer, J.; Freund, H.-J. *J. Catal.* **2004**, *226*, 88−100.
(11) Miyata, H.; Fujii, K.; Ono, T.; Kubokawa, Y.; Ohno, T.; Hatayama, F. *J. Chem. Soc., Faraday Trans. 1* **1987**, *83*, 675−685.
(12) Weckhuysen, B. M.; Keller, D. E. *Catal. Today* **2003**, *78*, 25−46.
(13) Wachs, I. E. *Catal. Today* **1996**, *27*, 437−455.
(14) Turek, A. M.; Wachs, I. E. *J. Phys. Chem.* **1992**, *96*, 5000−5007.
(15) Deo, G.; Wachs, I. E. *J. Phys. Chem.* **1991**, *95*, 5889−5895.
(16) Wachs, I. E. Personal communication.
(17) Magg, N.; Giorgi, J. B.; Schroeder, T.; Bäumer, M.; Freund, H.-J. *J. Phys. Chem. B* **2002**, *106*, 8756−8761.
(18) Perdew, J. P. In *Electronic Structure of Solids '91*; Ziesche. P., Eschrig H., Eds.; Berlin: Akademie Verlag GmbH, 1991.
(19) Perdew, J. P.; Chevary, J. A.; Vosko, S. H.; Jackson, K. A.; Pederson, M. R.; Singh, D. J.; Fiolhais, C. *Phys. Rev. B* **1992**, *46*, 6671−6687.
(20) Blöchl, P. E. *Phys. Rev. B* **1994**, *54*, 17953−17979.
(21) Kresse, G.; Joubert, D. *Phys. Rev. B* **1999**, *59*, 1758−1775.
(22) Monkhorst, H. J.; Pack, J. D. *Phys. Rev. B* **1976**, *13*, 5188−5192.
(23) Kresse, G.; Hafner, J. *Phys. Rev. B* **1993**, *48*, 13115−13118.
(24) Kresse, G.; Furthmüller, J. VASP 4.6.12. *Phys. Rev. B* **1996**, *54*, 11169−11186.
(25) Ganduglia-Pirovano, M. V.; Sauer J. *Phys Rev. B* **2004**, *70*, 045422.
(26) Blöchl, P. E.; Jepsen, O.; Andersen O. K. *Phys. Rev. B* **1994**, *49*, 16223−16233.
(27) Flükiger, P.; Lüthi, H. P.; Portmann, S.; Weber, J. *MOLEKEL 4.2*, 2000−2002.
(28) Portmann, S.; Lüthi, H. P. *Chimia* **2002**, *54*, 766−770.
(29) Nielsen, U. G.; Boisen, A.; Brorson, M.; Jacobsen, C. J. H.; Jakobsen, H. J.; Skibsted, J. *Inorg. Chem.* **2002**, *41*, 6432−6439.
(30) Brázdová, V.; Ganduglia-Pirovano, M. V.; Sauer, J. *Phys. Rev. B* **2004**, *69*, 165420.
(31) Karakida, K.-I.; Kuchitsu, K. *Inorg. Chim. Acta* **1975**, *13*, 113−119. Observed distance in $VOCl_3$ is 1.57 Å.
(32) Enjalbert, R.; Galy, J. *Acta Crystallogr. Sect. C* **1986**, *42*, 1467.
(33) Barker, A. S., Jr. *Phys. Rev.* **1963**, *132*, 1474−1481.
(34) Kirfel, A.; Eichhorn, K. *Acta Crystallogr. Sect. A* **1990**, *46*, 271−284.
(35) $[\Sigma_{i=1}^{N}(\Delta\nu_i)^2/N]^{1/2}$, N is the number of normal modes and $\Delta\nu_i$ is the difference between a calculated and a measured frequency.
(36) Adamo, C.; Barone, V. *J. Chem. Phys.* **1998**, *108*, 664.
(37) Tao., J.; Perdew, J. P.; Staroverov, V. N.; Scuseria, G. E. *Phys. Rev. Lett.* **2003**, *91*, 146401.
(38) Scott, A. P.; Radom, L. *J. Phys. Chem.* **1996**, *100*, 16502−16513.
(39) Clauws, P.; Broeckx, J.; Vennik, J. *Phys. Stat. Sol. (b)* **1985**, *131*, 459−473.
(40) Jaeger, R. M.; Kuhlenbeck, H.; Freund, H.-J.; Wuttig, M.; Hoffmann, W.; Franchy, R.; Ibach, H. *Surf. Sci.* **1991**, *259*, 235−252.
(41) Klimenkov, M.; Nepijko, S.; Kuhlenbeck, H.; Freund, H.-J. *Surf. Sci.* **1997**, *365*, 66−76.
(42) Stierle, A.; Renner, F.; Streitel, R.; Dosch, H.; Drube, W.; Cowie, B. C. *Science* **2004**, *303*, 1652−1656.